AUTHOR'S PROOF!

Theor Appl Climatol
DOI 10.1007/s00704-017-2193-7

ORIGINAL PAPER

Rainfall intensity patterns derived from the urban network of Barcelona (NE Spain)

Xavier Lana[1] · **C. Serra**[1] · **M. C. Casas-Castillo**[1] · **R. Rodríguez-Solà**[1] · **A. Redaño**[2] · **A. Burgueño**[2]

Received: 7 July 2016 / Accepted: 4 June 2017
© Springer-Verlag GmbH Austria 2017

Abstract An analysis of the normalised rainfall intensity curves in Barcelona (NE Spain) has been undertaken from 41 selected rain rate episodes recorded by an urban network of tipping buckets applying a 5-min integration time along the years 1994–2009. These curves, based on cumulative amount and time distributions, are modelled by a power law, this fact suggesting fractal behaviour. Four parameters characterise these curves. One of them is the exponent of the power law. Another one quantifies the intermittency of the rainfall along the episode. The other two are the coordinates of cumulative amount and time distribution from which the power law fits well the normalised curve. The total rainfall amount of the episode, its length and the coefficient of variation of the 5-min amounts are also considered as complementary parameters. Taking advantage of these seven parameters, patterns of rainfall intensity are determined for every episode. These patterns, together with the statistical distribution of 5-min amounts, maximum intensity and rainfall intermittence, should increase the knowledge on the urban rainfall regime with the aim of improving drainage design. In addition to present results, flood prevention should be complemented with extreme value analyses and quantification of return periods.

✉ Xavier Lana
francisco.javier.lana@upc.edu

[1] Departament de Física, Universitat Politècnica de Catalunya, Barcelona, Spain

[2] Departament de Física Aplicada—Meteorologia, Universitat de Barcelona, Barcelona, Spain

1 Introduction

Cumulative amount and time distributions of rainfall intensity permit the derivation of the normalised rainfall intensity curve, NIC, which characterise the rainfall intensity regime. In the present manuscript, NICs are obtained for the rain rate gauges pertaining to the urban network in Barcelona (NE Spain), a large city on the western Mediterranean coast (Lorente and Redaño 1990; Casas et al. 2010; Rodríguez et al. 2013a). The rainfall intensity is recorded by tipping bucket gauges, with an integration time depending on the rain rate. To permit a common uniform integration time, the measured intensities are converted to amounts recorded in 5-min intervals. The concept of the NIC is similar to the normalised rainfall curves, NRC, which relate the cumulative amount and time distributions at daily, monthly and annual rainfall amounts. These curves have been applied to different regions in the world (i.e. Ananthakrishnan and Soman 1989; Soman and Krishna 1990; Martín-Vide 2004; Burgueño et al. 2004, 2005; Alijani et al. 2008; Burgueño et al. 2010; Martínez et al. 2012), as well as at a global scale (Monjo and Martin-Vide 2016).

The main objectives of this research are the following: First, NIC are generated, and their properties are analysed for every one of the 23 rain rate gauges of the network. A power law is found to describe the relationship between cumulative 5-min rain amount distribution, $X(I)$, and the cumulative number distribution of these 5-min intervals, $Y(I)$. Significant correlations are established among several parameters of every rain rate episode and the respective NIC. These are the coefficient of variation, CV_I, of the 5-min rain amounts of every episode, the exponent κ of the power law concerning every NIC and coordinates X_m and Y_m defining the shortest percentages of $X(I)$ and $Y(I)$ from which an empiric NIC curve

UNCORRECTED PROOF

AUTHOR'S PROOF!
JnlID 704_ArtID 2193_Proof# 1 - 11/06/2017

fits well a power law. Additionally, the percentage Y_0 of 5-min intervals, with rain amounts null or below the rain measurement resolution, is also taken into account as a quantification of the rain intermittency along the episode. Two descriptive parameters, total rain amount, R, and episode length, L, have been also considered.

Second, as a complementary point of view of the obtained NIC patterns, whatever the rain rate gauge considered, it is verified that 5-min rain amounts are statistically well fitted to a Weibull distribution, with parameters estimated for every rain rate gauge by means of L-moments, taking advantage of their unbiased estimation and robustness to the presence of outliers in the dataset (Hosking and Wallis 1997). The respective scale, shape and location parameters are slightly different for every rain rate gauge. Then, local scale effects of topographic and geographic patterns on the rainfall intensity regime, such as vicinity of some gauges to the littoral chain or to the coast line, should not be discarded. Additionally, different synoptic situations associated with rainfall episodes could lead to slightly different rain rate patterns. Likely, distinctions could be made among the different meteorological situations producing the rainfall episodes, as eastern advections, frontal passages and convective phenomena.

The results derived from the NIC analysis and the statistical distribution of 5-min rain amounts, complemented with analysis based on space–time behaviour of intensity maxima, should be useful for improvements on the drainage system of Barcelona City and the surrounding metropolitan area, diminishing in this way the risk of floods. It should be remembered that this area has a Mediterranean rainfall regime, with an annual average of 617.7 mm/year and a standard deviation of 150.3 mm/year, in agreement with Fabra Observatory records (Barcelona) for the period 1917–2009. Nevertheless, the number of heavy rainfall episodes is not negligible, usually linked to very active eastern advections in autumn or convective phenomena in summer, and sometimes characterised by notable peaks of rainfall intensity. For example, after a close look at Fabra Observatory records within the mentioned recording period, close to 100 daily episodes ranging from 60.0 to 173.7 mm/day are detected. More details concerning the Fabra Observatory rainfall regime at annual, monthly and daily scale can be found in Lana et al. (2003, 2005), Burgueño et al. (2004), Casas et al. (2004, 2011) and Rodríguez-Solà et al. (2016), among others. It is also worth mentioning that a complete statistical analysis on quasi-instantaneous rainfall intensity in Fabra Observatory was achieved some years ago from measurements obtained with a Jardí rain rate gauge along 49 years (Burgueño et al. 1987, 1988, 1990; Vilar et al. 1988, 1991), with the aim of contributing to the design of microwave communications in terrestrial or earth–space radio links, where rain rate attenuation is meaningful. These statistics included the 5-min integration time rain rate distribution (Burgueño et al. 1988).

The contents of the paper are organised as follows. Section 2 (Database) briefly describes the instrumental characteristics of the urban network and its spatial distribution. The main characteristics of the selected 41 rainfall episodes are also summarised. Section 3 (Normalised Curves theory) introduces the concepts and mathematical formulation concerning the NIC, as well as the set of parameters characterising every one of the NIC. In the same section, the L-moments are introduced, which permit a straightforward selection of the best statistical model, and the Weibull distribution function is briefly introduced. Section 4 (Results) summarises the results obtained for the 41 episodes. A more detailed description of results concerning two rainfall episodes, as an example of possibilities offered by the analysis of intensity peaks, is also developed. Section 5 (Conclusions) summarises the main results and suggests new points of view for future studies of return periods concerning extreme intensities, with the main objective of reducing risks associated with floods in urban domains.

2 Dataset

Nowadays, the urban area of Barcelona, of 100 km^2 approximately, has a dense network of 23 tipping bucket rain rate gauges, brand Geónica S. A., with a 400-cm^2 collector funnel and a rain rate resolution of 0.1 mm/5 min (Casas et al. 2010; Rodríguez et al. 2013a), in operation since 1994 (Fig. 1; Table 1). From the recordings of this network until 2009, 5-min rainfall series have been derived for every gauge. The topography of the urban area (Fig. 1) is characterised by a low hill (150 m a.s.l.) close to the harbour, with a steep slope faced to the coast, and a relatively flat area extending from the coast line to the foot of the littoral chain, which gets altitudes of up to 500 m a.s.l.

All the selected rainfall episodes have been recorded on at least one rain rate gauge of the urban network, satisfying the additional constraints:

- The rainfall amounts have return periods longer than or equal to 1 year for any of the durations ranging from 5 min to 24 h (Casas et al. 2004, 2010).
- Given that NIC analysis requires a high number of 5-min amounts, only episodes with lengths longer than or equal to 2 h have been considered.

After applying these two constraints, 41 episodes have been chosen. Conditions to define the recording length of an episode at every gauge of the network are also applied in order to consider the different start and ending times for the same episode at the different gauges. These conditions are as follows:

UNCORRECTED PROOF

AUTHOR'S PROOF!

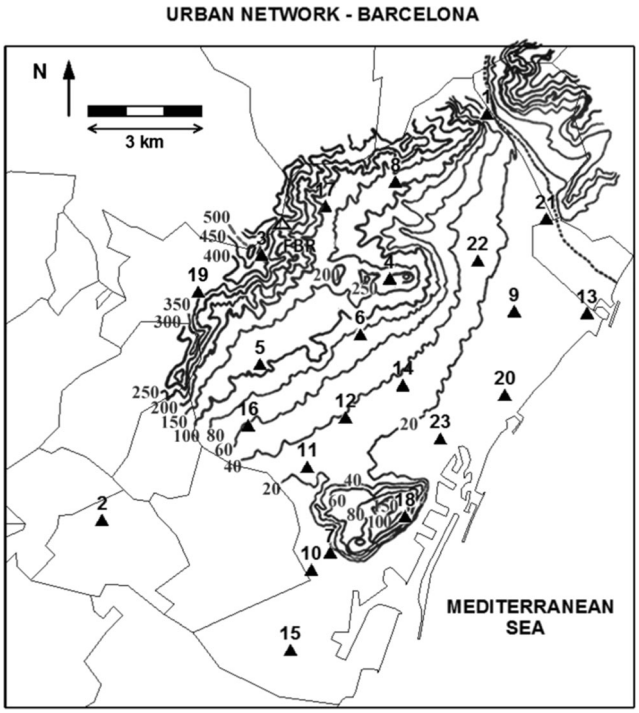

Fig. 1 Urban network of 23 tipping bucket rain rate gauges of Barcelona (*solid triangles*). The Jardí rain rate gauge of Fabra Observatory is indicated by an *open triangle*. *Topographic contour lines* for the urban area are also included

Q5 – The recording of an episode in a gauge starts with a 5-min amount exceeding or equalling 0.1 mm/5 min, provided that this threshold has not been exceeded at least 1 h before.
– The recording of an episode in a gauge finishes when a waiting time longer than 1 h is detected after the last 5-min amount exceeding or equalling 0.1 mm/5 min.

Then, episodes recorded in a rain gauge can include several 5-min intervals with amounts below the rain rate resolution, shorter than 1 h. These intervals are named rainfall intermittences. It is also worthy of mention that the recorded rain amount of an episode in a gauge is not a criterion to accept or reject these rain rate data.

NIC for integration times longer than 5 min would be also possible. Nevertheless, a relevant shortcoming has to be considered: the number of samples to build up the NIC of a rainfall episode decreases with longer integration times. Consequently, the accuracy of empiric NIC at longer than 5-min integration time would be debatable.

As a description of the selected 41 episodes measured by the urban network, their dates and coefficients of variation, obtained as the quotient of the standard deviation and the average of 5-min amounts, together with the average total amount and average length, are summarised in Table 2. The sample of rainfall episodes includes relatively short (148.0 min) as well as long (1445.5 min) episodes, with a wide range of rain amounts ranging from a small amount of 6.2 mm to a high amount of 102.0 mm. Most of CV_I are constrained to a narrow range of values close to 1.0, suggesting a moderate dispersion of 5-min rain amounts. Nevertheless, five episodes are associated with CV_I exceeding 2.0, being detected in these cases a higher irregularity of the 5-min amounts. Data included in Table 2 permit the assignment Q6 of 10 episodes to spring, 3 to summer, 18 to autumn and 10 to winter.

The variety and complexity of the 5-min rain amount patterns are illustrated with two examples in Fig. 2. Both examples correspond to the beginning of autumn (September 29, 1994, and October 17, 1999), recorded at gauges 2 and 1, respectively. A straightforward revision of Fig. 2 evidences the very different profiles of both episodes. Whereas the first episode is characterised by an amount of 66.4 mm and a length of 425 min, the second achieves an amount of 24.3 mm and a shorter length of 250 min. Time evolutions of both episodes are very different. The first one is characterised by a low degree of precipitation intermittency and a moderate set of intensity peaks, never exceeding 3.3 mm/5 min. Conversely, the rainfall amount of the second episode is basically generated by a narrow and isolated intensity peak achieving 7.4 mm/5 min and a high degree of rainfall intermittency. In agreement with daily surface and 500-hPa charts obtained from *www.meteoffice.gov.uk* and *www.netweather.tv*, the first episode

Q3 t1.1 t1.2 Q4 t1.3 t1.4 t1.5 t1.6 t1.7 t1.8 t1.9 t1.10 t1.11 t1.12 t1.13 t1.14 **Table 1** Altitude above sea level, Z, and universal transverse mercator, UTM, coordinates for the 23 gauges of the urban network and the Fabra Observatory, FBR

Gauge	Z (m)	X (UTM)	Y (UTM)	Gauge	Z (m)	X (UTM)	Y (UTM)
1	18	432572	4590189	13	5	435184	4584975
2	15	422530	4579549	14	32	430373	4583077
3	450	426690	4586494	15	3	427443	4576149
4	162	430034	4585878	16	67	426341	4582030
5	120	426648	4583627	17	206	428357	4587775
6	86	429270	4584410	18	146	430431	4579649
7	9	428485	4578698	19	293	425042	4585529
8	148	430181	4588414	20	3	433035	4582822
9	7	433279	4585023	21	14	434117	4587439
10	4	427987	4578247	22	26	432334	4586332
11	27	427879	4580946	23	8	431351	4581678
12	37	428911	4582279	FBR	415	426783	4585860

UNCORRECTED PROOF

AUTHOR'S PROOF!

Q7 **Table 2** Basic characteristics of every one of the 41 rainfall episodes recorded at 23 rain gauges

Y/M/D	CV_I	R (mm)	L (min)	Y/M/D	CV_I	R (mm)	L (min)	Y/M/D	CV_I	R (mm)	L (min)
94/09/29 (1)	0.87	63.6	425.4	98/01/27 (15)	1.63	18.0	342.4	06/01/30 (29)	1.37	7.9	406.9
94/10/19 (2)	1.66	48.8	322.5	98/09/23 (16)	1.42	13.0	250.9	06/08/15 (30)	2.12	18.3	148.3
96/01/29 (3)	1.42	43.6	1445.5	98/12/02 (17)	0.96	102.0	1231.1	06/09/12 (31)	2.23	10.7	167.4
96/04/17 (4)	0.76	49.0	357.3	99/10/17 (18)	2.16	33.2	257.5	06/09/14 (32)	1.56	16.3	286.5
96/05/11 (5)	0.66	8.4	255.5	00/09/28 (19)	1.60	25.3	208.0	07/04/02 (33)	1.47	20.5	400.5
96/05/11 (6)	1.43	31.3	517.4	02/07/31 (20)	1.65	85.3	483.6	07/04/02 (34)	1.71	33.1	450.2
96/06/02 (7)	0.96	51.0	675.9	02/10/08 (21)	1.49	92.8	663.7	07/10/26 (35)	1.91	35.2	595.0
96/10/13 (8)	1.35	11.0	230.7	04/09/03 (22)	2.30	19.9	204.4	08/05/09 (36)	0.84	11.9	291.2
96/10/14 (9)	1.74	90.1	1388.5	05/10/12 (23)	1.08	85.6	333.1	08/05/09 (37)	0.86	6.2	306.2
97/01/28 (10)	1.32	32.7	406.8	05/11/09 (24)	1.39	20.0	338.0	08/05/10 (38)	1.35	38.2	725.0
97/04/19 (11)	1.41	31.0	598.4	05/11/13 (25)	1.76	23.2	493.6	09/09/20 (39)	1.66	20.3	211.9
97/04/20 (12)	1.25	12.4	676.8	06/01/27 (26)	0.60	22.5	661.0	09/10/21 (40)	1.21	17.0	285.7
97/12/16 (13)	1.73	36.8	427.6	06/01/28 (27)	0.66	6.7	294.3	09/10/22 (41)	1.47	53.8	386.8
98/01/26 (14)	1.35	9.9	256.9	06/01/29 (28)	2.26	21.2	459.8				

CV_I, R, and L design the coefficient of variation, averaged amount and averaged length for every episode. Y/M/D refers to year, month, and day, respectively, of the data beginning for every episode. Together with dates, episode numbers are included within parentheses

UNCORRECTED PROOF

would be generated by low pressures at the south of the Iberian Peninsula and north of Africa, together with an anticyclone covering Azores Islands and central and eastern Europe. Under these synoptic conditions, the littoral coast in Barcelona and surrounding areas would be submitted to an eastern advection, being recorded a notable daily amount, partially favoured by conditions at the 500-hPa level. The second episode, less relevant than the first, would be a consequence of a low-pressure nucleus on the Atlantic Ocean, close to the northwest of the Iberian Peninsula. Relatively cold air masses in the vicinity of the Mediterranean coast, in agreement with the 500-hPa-level chart, would contribute to this episode with a non-negligible daily rain amount.

Notable differences among the 41 episodes are found from the viewpoint of rain amounts, length, rain intermittency and intensity peaks. Nevertheless, relationships between NIC parameters, as well as the existence of a single mathematical formulation (a power law) for all the episodes, permit the establishment of common patterns on the rainfall intensity regime, whatever the season and synoptic situations related to the rainfall episodes.

3 Mathematical formulation and concepts

3.1 Normalised rainfall intensity curves

The NIC for every rainfall episode are based on two empirical distributions. The first one is the cumulative amount distribution, $X(I)$, which is defined as

$$X(I) = Prob(i \le I) = \frac{Rain\ amount\ \text{due to 5-min}\ intervals\ with\ intensities \le I}{Total\ rain\ amount\ of\ the\ episode} \quad (1)$$

where i represents the set of 5-min rain amounts less than or equal to a threshold I. The second is the cumulative time distribution, $Y(I)$, which is defined as

$$Y(I) = Prob(i \le I) = \frac{Number\ of\ \text{5-min}\ intervals\ with\ intensity \le I}{Total\ number\ of\ \text{5-min}\ records} \quad (2)$$

It has to be taken into account that Eqs. (1) and (2) may include null records (due to rainfall intermittency) and inappreciable intensities due to rain rate gauge resolution. According to Ananthakrishnan and Soman (1989), Jolliffe and Hope (1996) and Burgueño et al. (2004), a possible mathematical relationship between $X(I)$ and $Y(I)$ to describe the NIC would be

$$X(I) = Y(I)\exp\{-b[1-Y(I)]^c\} \quad (3)$$

Nevertheless, some previous tests have proved that, conversely to NRC, NIC do not fit well with Eq. (3), and a better solution is to consider a power law with some constraints and new parameters, with respect to those derived from Eq. (3). The power law proposed is

$$Y(I) \propto X(I)^{\kappa};\quad X(I) \ge X_m \quad (4)$$

with X_m being the lowest percentage of 5-min rain amount for which Eq. (4) is accomplished, and $Y_m \propto X_m^{\kappa}$, the corresponding percentage of 5-min intervals. After revising the results for the 41 episodes, it is observed that Y_m includes 5-min intervals with records below the rain rate gauge resolution, corresponding to rainfall intermittence, Y_0, and a few 5-min records slightly exceeding the rain rate resolution of 0.1 mm/5 min. Consequently, it is expected that X_m usually reaches small values.

AUTHOR'S PROOF!

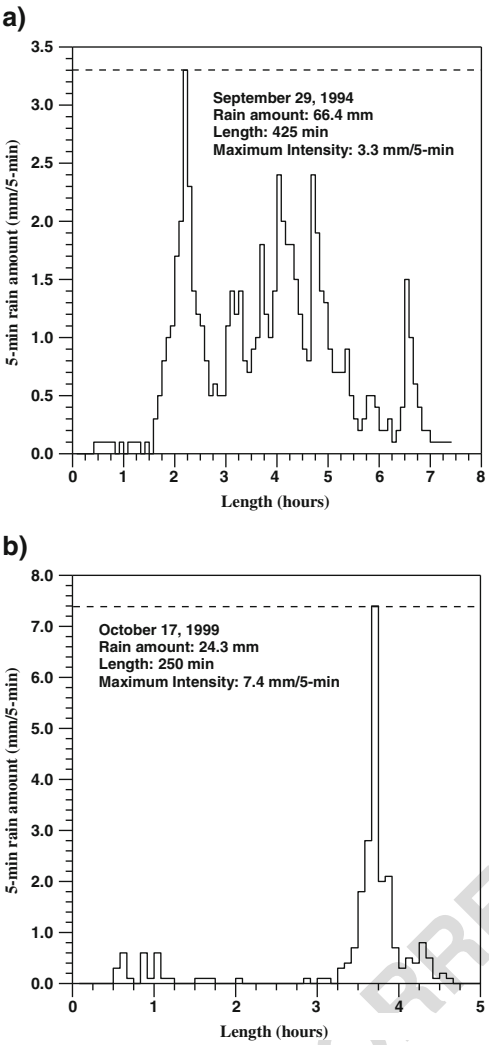

Fig. 2 **a** The 5-min rain amounts recorded in gauge number 2 on *September 29, 1994*, with notable rain collected and several intensity peaks. **b** The 5-min rain amounts recorded in gauge number 1 on *October 17, 1999*, with a moderate rain amount but with a single intensity peak

A rainfall episode will be described by the following parameters: on the one hand, three basic magnitudes which quantify rain amount R (mm), length L (min) and CV_I of the episode; on the other hand, four additional parameters directly related to NIC. They are the exponent κ of the power law of Eq. (4), the coordinates (X_m,Y_m) defining the lowest percentage of rain amount and 5-min intervals for which the power law is valid and, finally, the coordinate Y_0, established as the percentage of 5-min intervals with records below the rain rate gauge resolution, thus quantifying the degree of intermittency of the rainfall episode. The exponent κ can be determined by a linear regression of empiric data representing Eq. (4) at logarithmic scale. The algorithm proposed by Malamud and Turcotte (1999) is applied for a more accurate estimation of κ. After that, X_m, Y_m and Y_0 are immediately derived. Parameters R, L and CV_I are also found for every episode at the different gauges.

3.2 L-moments and Weibull distribution of 5-min rain amounts

Besides description and quantification of every rainfall episode in terms of the NIC, additional valuable information can be obtained by analysing the statistical distribution of all the 5-min rain amounts recorded on every rain rate gauge for the 41 episodes. In this way, it can be established if there are relevant differences on the 23 rain rate gauges of the urban network, perhaps as a consequence of their vicinity to the littoral chain or to the Mediterranean coast.

The best theoretical distribution function has been chosen following three steps. First, the L-moments (Hosking and Wallis 1997) are applied to select a theoretical distribution function. This theoretical function has to offer the best fit between empiric L-skewness, τ_3, and L-kurtosis, τ_4, moments and those corresponding to the chosen function. In agreement with this requirement, the best function for the 5-min amounts would be the Weibull distribution

$$F(x) = 1-\exp\left[-\{(x-\zeta)/\theta\}^{\delta}\right] \quad ; \quad \zeta \le x < \infty \tag{5}$$

Second, location, ζ, scale, θ, and shape, δ, parameters are given by Hosking et al. (1985) as

$$\delta \approx \left\{7.8590C + 2.9554C^2\right\}^{-1} = 1/\mu \tag{6a}$$

$$C = \frac{2}{3+\tau_3} - \frac{\log 2}{\log 3} \tag{6b}$$

$$\theta = \frac{\lambda_2}{(1-2^{-\mu})\Gamma(1+\mu)} \tag{7}$$

where λ_2 is the second-order L-moment and $\Gamma(\cdot)$ the complete gamma function, and

$$\zeta = \lambda_1 + \theta\ \Gamma(1+\mu) \tag{8}$$

with λ_1 being the first-order L-moment. Then, a specific Weibull distribution is obtained for every set of 5-min empiric data. And third, the goodness of fit between empiric and theoretical distribution functions is assessed by means of the Kolmogorov–Smirnov test (Benjamin and Cornell 1970). If the empiric distribution function is within 95% confidence bands determined by this test, the Weibull model is finally accepted.

4 Results

NIC are obtained taking advantage of the 41 selected rainfall episodes recorded at 23 rain rate gauges of the urban network, being noticeable that in all cases, the power law given by Eq. 4 is accomplished, with square regression coefficients above 0.96. The same rainfall episodes used as examples in Fig. 2

UNCORRECTED PROOF

AUTHOR'S PROOF!
JnlID 704_ArtID 2193_Proof# 1 - 11/06/2017

have been considered as examples of the fitting of the empiric NIC to a power law in Fig. 3. The first example (September 29, 1994, recorded by gauge number 1) is characterised by short intermittency and moderate intensity peaks. Additionally, its NIC is modelled by a parameter κ equal to 0.374 (with square regression coefficient of 0.99), with 72.5% of 5-min intervals ($Y_m = 0.275$) fitting well the NIC power law and contributing to 97.0% of the total rainfall of the episode ($X_m = 0.030$). In short, this would be an example of a rainfall episode with short intermittency (Y_0 close to 0.06) and then a relatively small number of records below the resolution of the rain rate gauge. The second example (October 17, 1999, recorded by gauge number 2) is quite different with respect to the percentage of 5-min rain amounts, given that only 35.4% of 5-min intervals fit well the NIC power law ($Y_m = 0.646$) but explain 93.9% of episode amount ($X_m = 0.061$). As expected, its parameter κ (0.175) is smaller than that corresponding to the first example, but the square regression coefficient is also very acceptable (0.98). Conversely to the first episode, larger intermittency (Y_0 close to 0.40) is detected, and higher intensity peaks are expected to explain a quite similar percentage of the episode amount, with less than half of 5-min rain amounts exceeding the resolution level of the rain rate gauge.

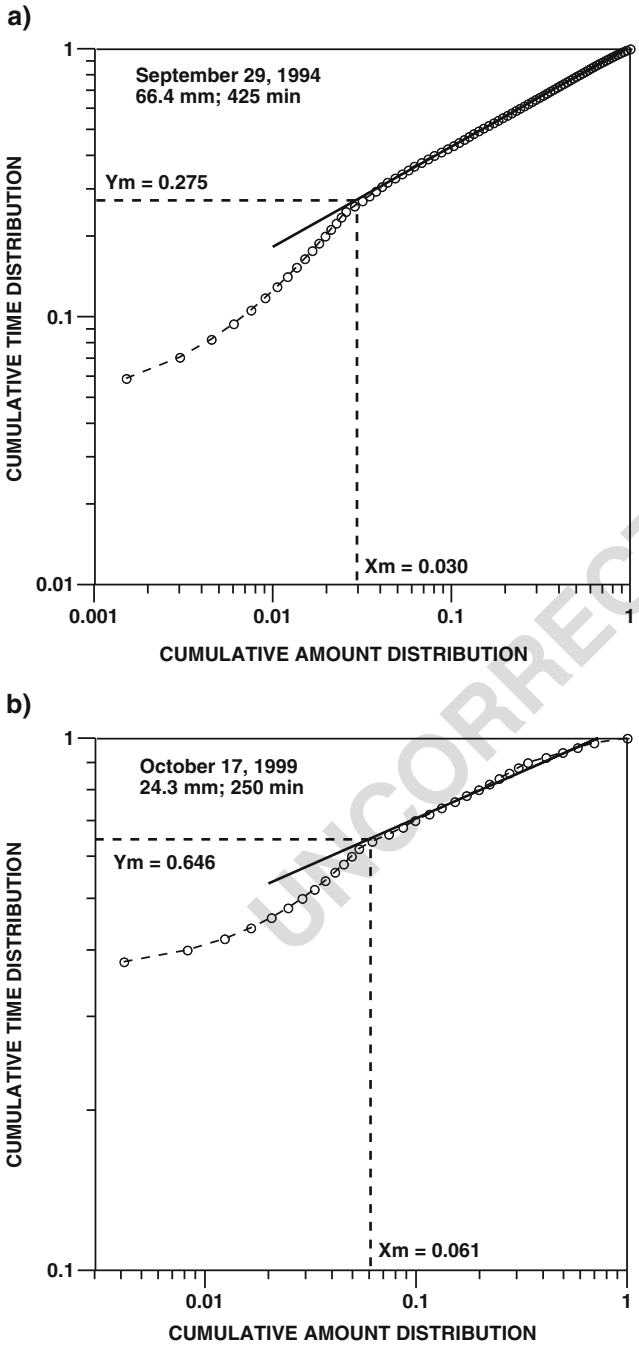

Fig. 3 Empiric NIC satisfying a power law for $X(I)$ above X_m for **a** *September 29, 1994* (rain gauge number 2), and **b** *October 17, 1999* (rain gauge number 1). *Open circles* represent empiric NIC, the *straight line* the power law fit in logarithmic scale and the *dashed lines* the (X_m,Y_m) coordinates

A global overview of the NIC behaviour is obtained by revising the most remarkable correlations between pairs of the parameters $\{CV_I, R, L, X_m, Y_m, Y_0, \kappa\}$. In agreement with Table 3, only pairs of parameters with cross-correlation exceeding 0.5 are taken into account. Additionally, in order to extract some conclusions and physical interpretations, the plots of Fig. 4 represent these correlations for the set of 41 rainfall episodes. Thus, correlations between parameters have to be interpreted as very probable behaviours of the 5-min rain amounts, but not as an exact relationship for every rainfall episode.

It has to be remembered that an almost absolute dependence of normalised curves on parameter CV_I is true for NRC but discarded for NIC after some empirical tests. In spite of this, some dependence of these normalised curves on CV_I is observed through the decreasing tendency of κ with increasing values of CV_I. Consequently, CV_I indirectly models the normalised curves. Figure 4a describes signs of κ depending on the logarithm of CV_I. According to this fact, modelling NICs in terms of the scaling exponent κ, in agreement with the well-known fractal scaling behaviour of rainfall intensities (Rodríguez et al. 2013b), would be more evident and useful than an interpretation

Table 3 Covariance between pairs of parameters describing the set of 41 rainfall episodes

	CV_I	R	L	X_m	Y_m	Y_0	κ
CV_I	1.0						
R	−0.049	1.0					
L	−0.122	*0.573*	1.0				
X_m	−0.361	*−0.527*	0.004	1.0			
Y_m	0.263	*−0.682*	−0.110	*0.713*	1.0		
Y_0	*0.567*	*−0.477*	−0.120	0.238	*0.806*	1.0	
κ	*−0.764*	0.204	0.210	0.128	*−0.529*	*−0.858*	1.0

Pairs in italic type correspond to cross-correlations exceeding 0.5

UNCORRECTED PROOF

AUTHOR'S PROOF!

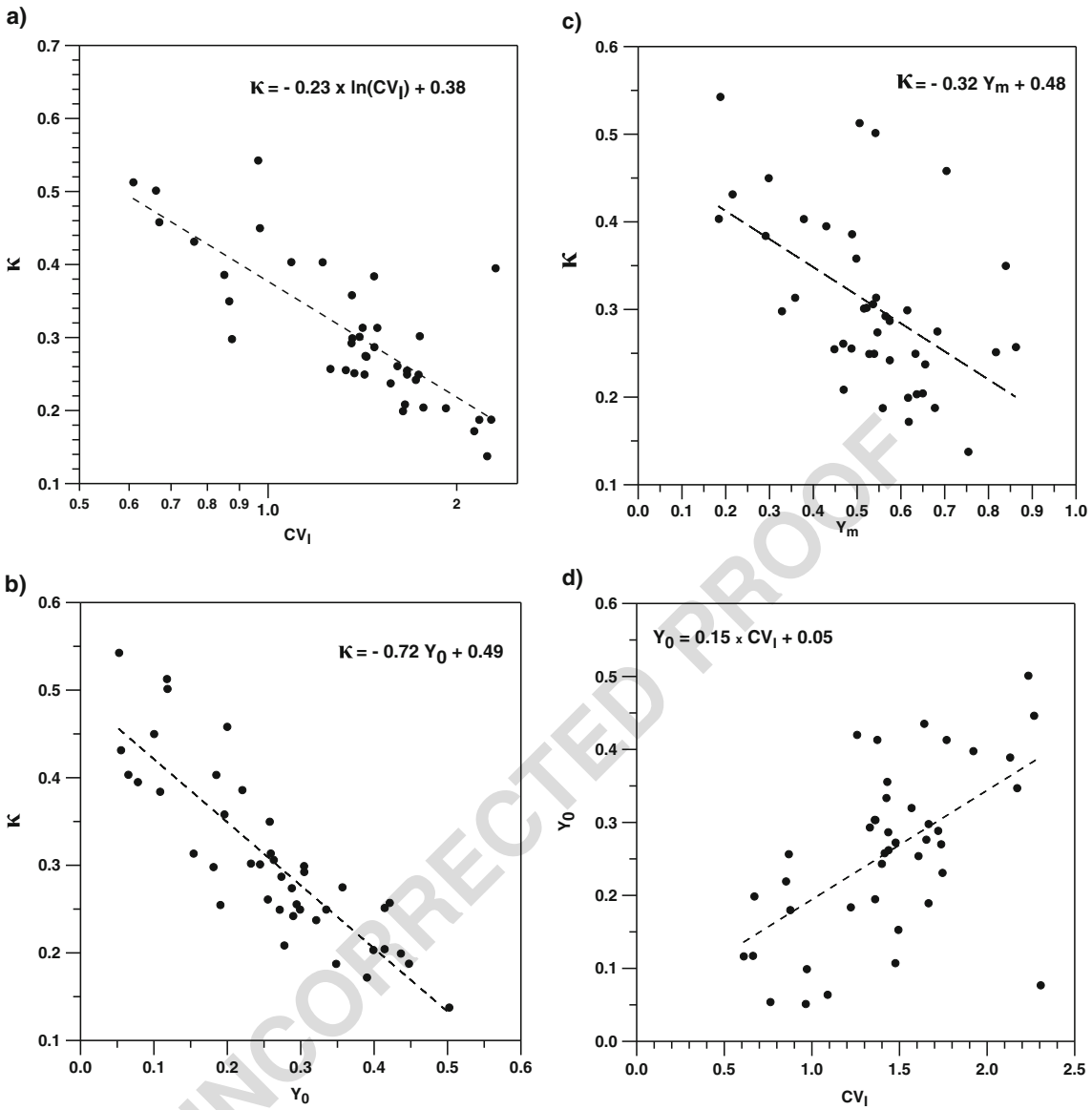

UNCORRECTED PROOF

Q8 **Fig. 4** Relationships between pairs of parameters characterising 5-min rain amount episodes. Only pairs of parameters with clear signs of dependence between them (bold characters in Table 3) have been considered. *Dashed lines* represent the different functions fitting roughly the observed values of the selected parameters

in terms of CV_I. Additionally, it is also worth mentioning the linear decreasing trend of κ with parameters Y_0 and Y_m (Fig. 4b, c). In this way, κ would be partially conditioned by rainfall intermittency.

The relationships (increasing linear trends) of Y_0 with CV_I and Y_m are represented in Fig. 4d, e. In agreement with these plots, an increase of the rainfall intermittency would be in concordance with an increase of CV_I or, in other words, with the dispersion of 5-min rain amounts. Once again, the linear behaviour is not well-accomplished for some CV_I close to 2.2–2.3. Taking into account the definition of coordinates (X_m,Y_m), associated with 5-min intervals with null or small rain amounts, an increasing trend of Y_0 for increasing Y_m was also expected.

The possible relationship between X_m, Y_m, L and R is shown in Fig. 4f. Instead of negligible rain amount and rainfall intermittency concepts, quantified by X_m and Y_m, their complementary quantities scaled to L and R have been plotted. The relationship between L and R would be described by a power law with an exponent equal to 0.58.

Figure 4g shows Y_m decreasing following a power law, while R increases. In other words, the higher the rainfall amount, the lower is the number of 5-min rain amounts out of the power law. Nevertheless, departures from this rule are observed for episodes achieving rain amounts above 50 mm. Similarly, in agreement with Fig. 4h, X_m decreases with R. In this case, the decreasing trend would be given by a power law (almost equivalent to a dependence on $1/R$). Finally, Fig. 4i

AUTHOR'S PROOF!
JnlID 704_ArtID 2193_Proof# 1 - 11/06/2017

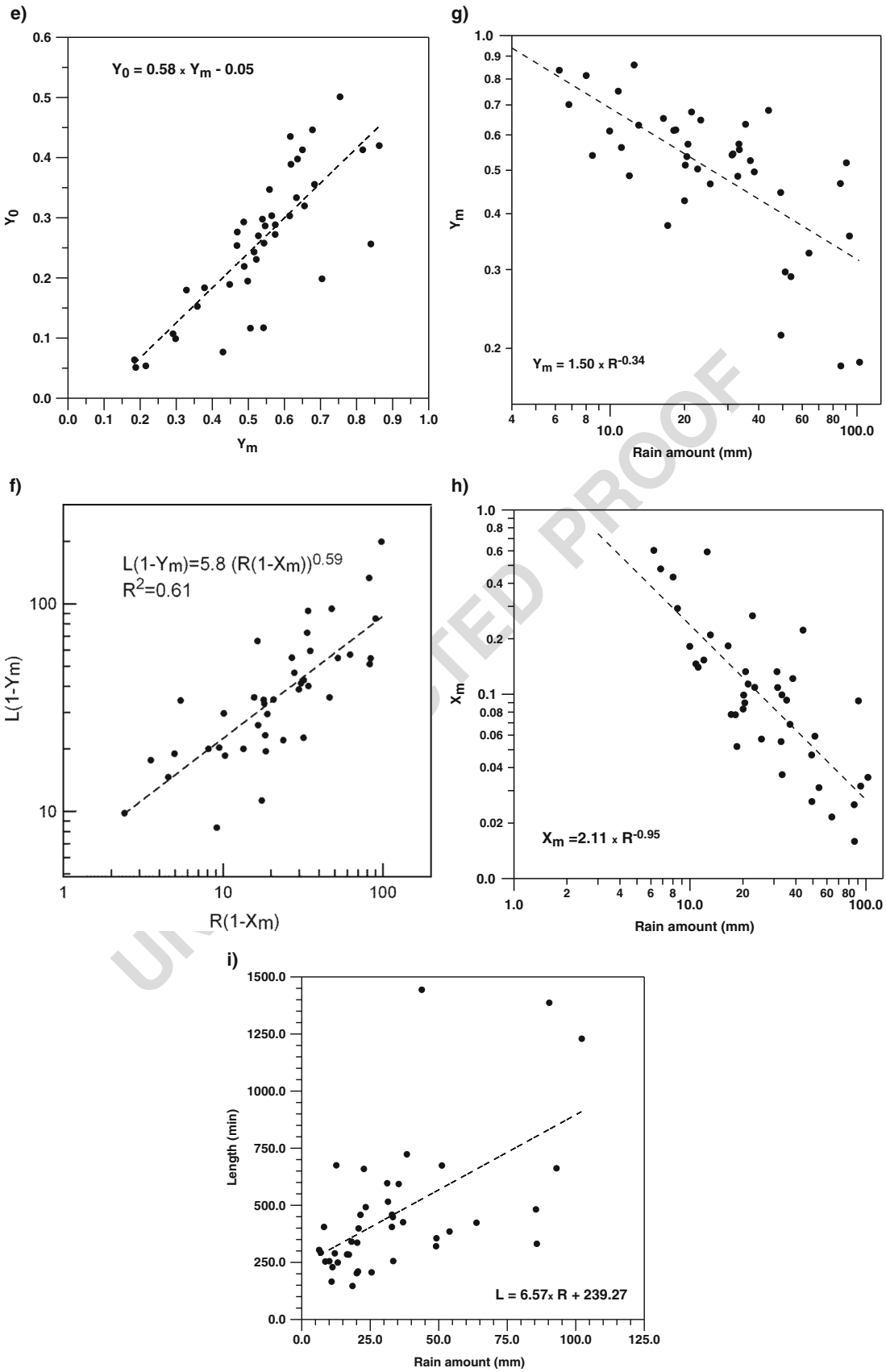

Fig. 4 (continued)

AUTHOR'S PROOF!

schematises another expected and quite evident dependence of R on L. The evolution is more or less linear, except for the longest episodes, with empiric values of R in disagreement with the expected mathematical model.

Pairs of empiric points are many times notably scattered around the mathematical function proposed to explain a possible relationship among them. Consequently, these functions can be assumed as mathematical models describing increasing or decreasing tendencies between pairs of parameters. A more detailed description is given by the histograms for the different parameters plotted in Fig. 5 for the whole set of episodes and gauges. Most of the NICs have lengths L ranging from 180 to 480 min and amounts R within the 5.0–40.0-mm range. Most of the irregularity degree, quantified by CV_I, fluctuates from 0.6 to 2.0, with a few very irregular episodes. According to the X_m histogram, most of the 5-min amounts are characterised by percentages below 15%, not accomplishing the NIC model. From the Y_m histogram, between 35 and 75% of 5-min intervals do not fit well the NIC model. Even though the upper limit of 75% seems to be excessively high, it has to be remembered that Y_m includes intermittence given by Y_0. Most intermittences are characterised by percentages between 0 (null intermittence) and 45% (very high intermittence). Finally, most of the power law exponents κ are within a narrow range from 0.20 to 0.35.

UNCORRECTED PROOF

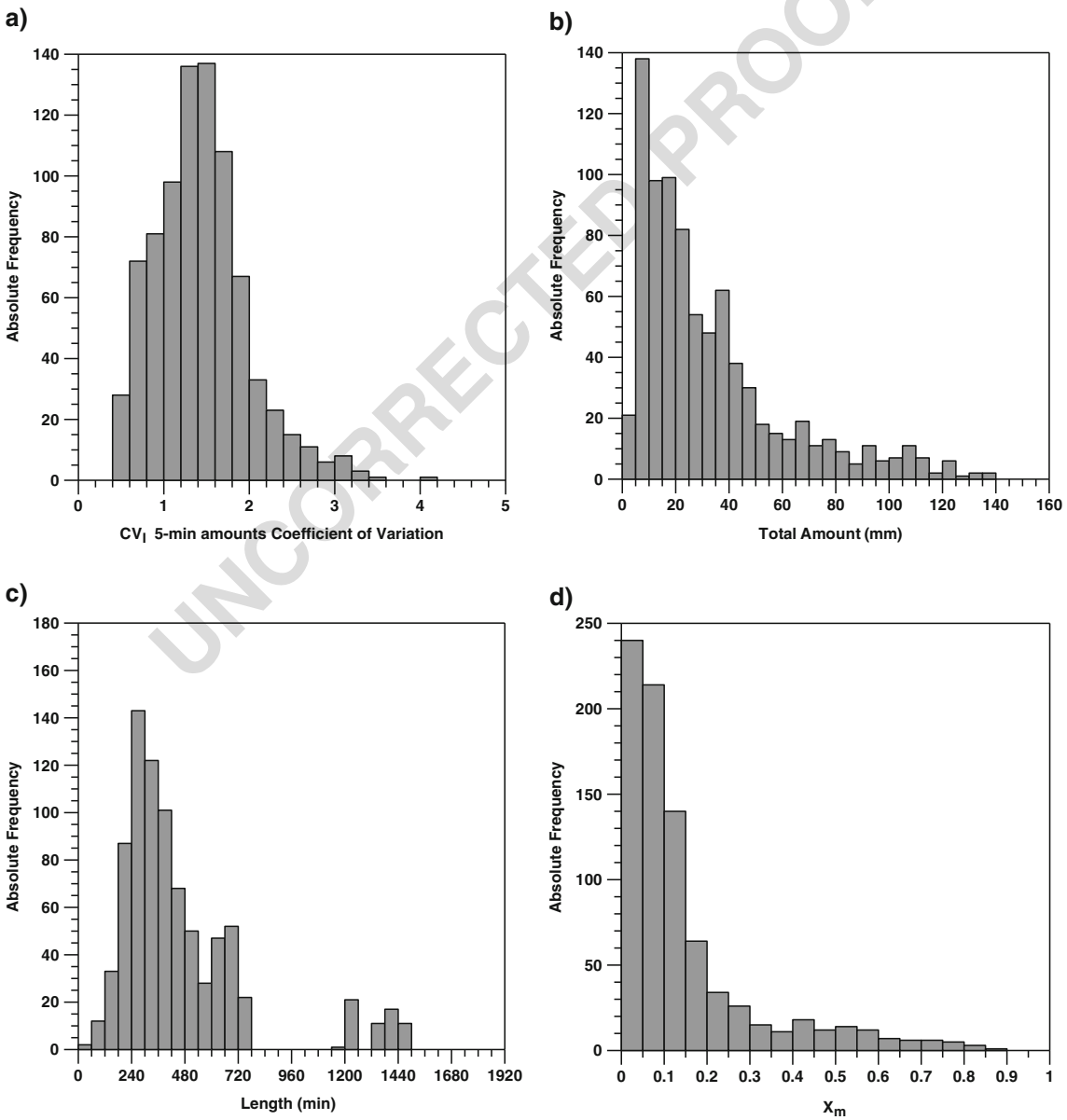

Fig. 5 Histograms of parameters **a** CV_I, **b** R, **c** L, **d** X_m, **e** Y_m, **f** Y_0 and **g** κ derived for the 41 episodes recorded at the different gauges. *Dashed lines* in Y_m and κ histograms correspond to gaussian distributions

AUTHOR'S PROOF!
JnlID 704_ArtID 2193_Proof# 1 - 11/06/2017

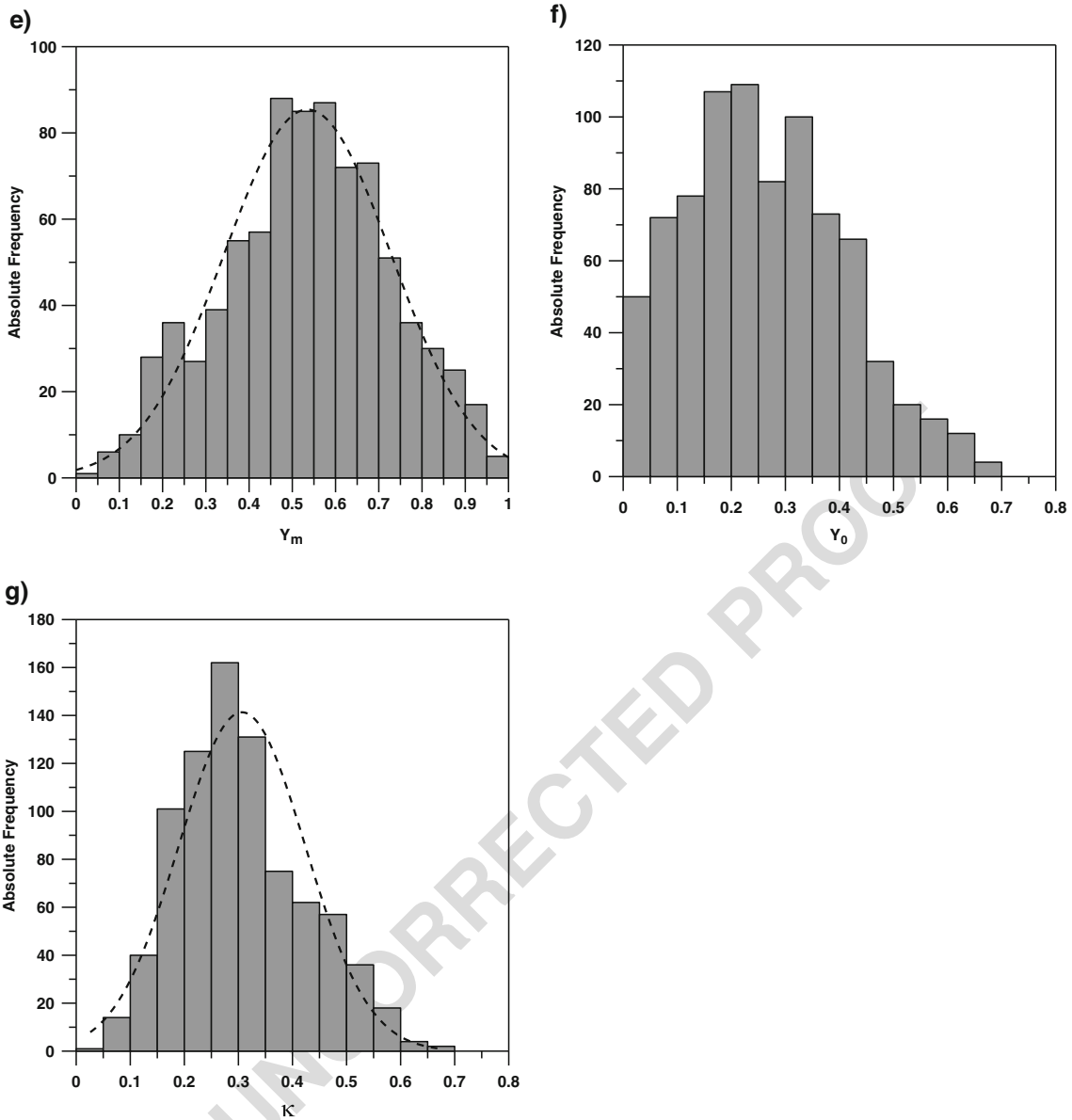

Fig. 5 (continued)

With respect to the cumulative amount distribution $X(I)$, the L-skewness–L-kurtosis graph of Fig. 6a shows evident signs of close vicinity to the Weibull function. The 23 empiric samples of L-skewness and L-kurtosis, taking into account all the 5-min rain amounts of the 41 episodes recorded at every rate rain gauge, are constrained to a narrow range (0.37–0.40 for L-kurtosis, 0.65–0.70 for L-skewness) close to the Weibull distribution line. Consequently, with minimum uncertainty, the hypothesis that 5-min rain amounts for every gauge are well-fitted to a single Weibull model can be assumed. Nevertheless, after applying Eqs. 6a–8, every one of the 23 sets of records is characterised by slightly different location, scale and shape parameters. Figure 6b, c describes the spatial distribution of scale, θ, and shape, δ, parameters. With respect to θ, three differentiated areas are detected. One of them, at the west of the urban area, is characterised by low values of θ. A similar pattern depicts a spatial fringe towards the NE of the urban area. Conversely, besides a small nucleus of high values of θ at the north, the main concentration of these high values is found at the south of the urban area, very close or inside Barcelona's harbour. The spatial distribution of δ depicts some differences with respect to θ. In spite of a concentration of low values of δ, again at the NE, similar places with high values of θ are now characterised by the lowest values of δ. A clear relationship between the spatial distribution of these Weibull parameters and the vicinity of rain gauges to the coast or to the littoral chain has not been found. In spite of this, a general agreement can be observed between the spatial patterns of both Weibull parameters (especially shape, δ) and the spatial clustering patterns for short rainfall durations obtained by

UNCORRECTED PROOF

AUTHOR'S PROOF!

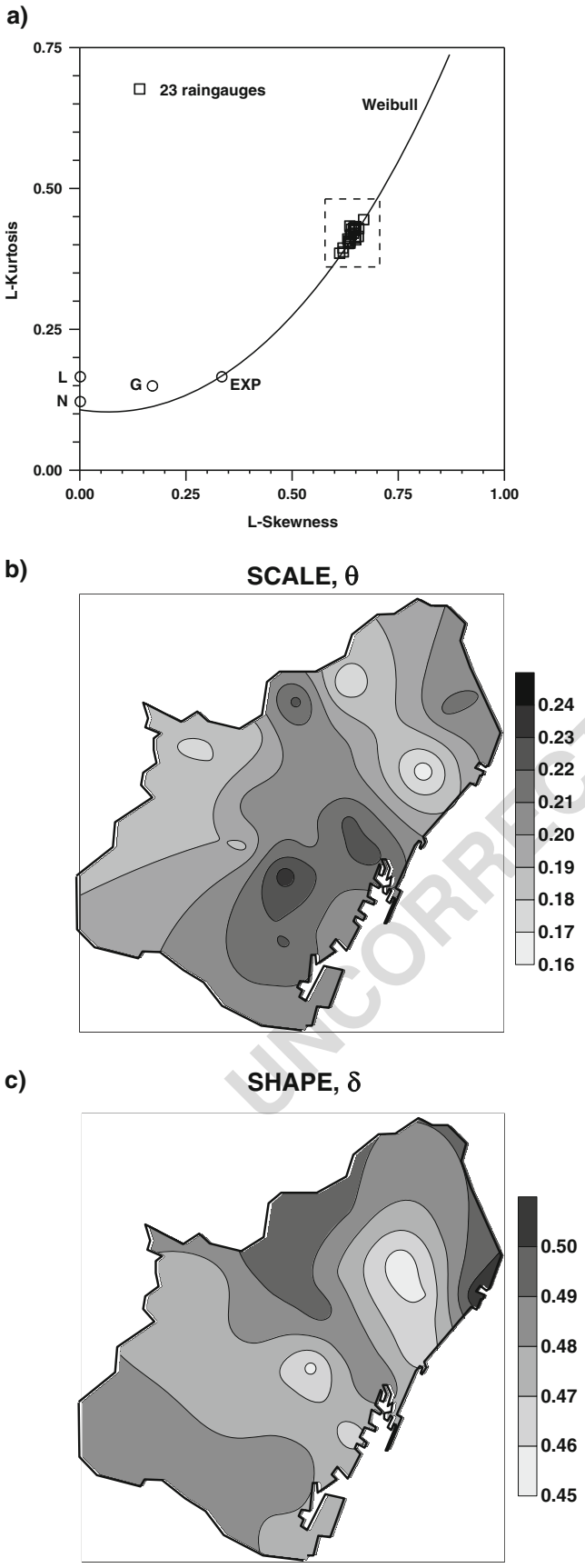

◀ **Fig. 6** **a** L-skewness–L-kurtosis diagram for the 23 series of 5-min rain amounts. *L*, *N*, *G*, and *E* correspond to logistic, normal, Gumbel and exponential cumulative distributions, respectively, whereas the *solid line* corresponds to the Weibull distribution. **b** Spatial distribution of the Weibull scale parameter. **c** Spatial distribution of the Weibull shape parameter

Rodríguez et al. (2013a), who studied the correlation among the intensities recorded by the different gauges of the urban network. Nevertheless, given that the recording period is relatively short and the number of episodes is not very high, these spatial patterns should be simply assumed as an approach to their spatial distributions. Finally, Fig. 7 shows an example of an empiric data fitting well the Weibull distribution for recordings of gauge number 1, showing the resulting Weibull distribution and the 95% confidence band according to the Kolmogorov–Smirnov test. Taking into account the high number of samples derived by 5-min intervals recorded for 41 episodes, the 95% confidence band has been quantified as $1.36/N^{1/2}$, with N being the number of samples (Benjamin and Cornell 1970). It has to be mentioned in this example of Weibull distribution that some discrepancies between theoretical and empiric data distributions are detected up to intensities close to 1.0 mm/5 min. Nevertheless, the empiric distribution is always within the Kolmogorov–Smirnov confidence band, and the fit could be assumed as almost perfect for intensities exceeding or equalling 1.0 mm/5 min. A very similar behaviour has been found for the remaining 22 Weibull distributions.

UNCORRECTED PROOF

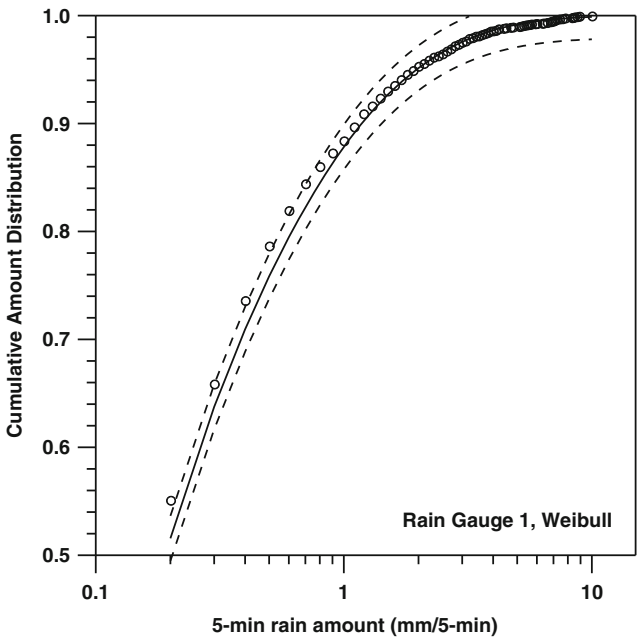

Fig. 7 An example of 5-min rain amounts cumulative distribution. *Open circles* and the *solid line* represent empiric and Weibull distributions, respectively. *Dashed lines* correspond to 95% confidence bands according to the Kolmogorov–Smirnov test

AUTHOR'S PROOF!
JnlID 704_ArtID 2193_Proof# 1 - 11/06/2017

Patterns of rainfall intensity recorded at the urban network are also complemented with some characteristics of 5-min rain amounts. The maximum intensity along an episode has been selected every 5 min from the 23 rain rate gauges, with $I_{5\text{-min}}$ being then generated as a series of maximum intensities for every episode. From these series, it is straightforward to obtain the maximum 5-min rain amount of every rain episode, $I_{\max}$, the average, I_m, of $I_{5\text{-min}}$ series and its standard deviation, I_σ, as well as the corresponding coefficient of variation, CV_{Imax}, for every episode.

Figure 8a–c shows clear linear increasing tendencies of $I_{\max}$ for increasing values of average, standard deviations and CV_{Imax} of $I_{5\text{-min}}$. As expected, it is confirmed that $I_{\max}$ would be larger for episodes with high I_m. Nevertheless, the linear increasing tendency with I_σ or CV_{Imax}, implying that wider ranges of I_m favours higher $I_{\max}$, was not so evident a priori. In agreement with the three previous figures, Fig. 8d also depicts a clear linear increasing trend for I_m in terms of I_σ. The two examples of maximum profiles are described in Fig. 9. In agreement with Fig. 2a, the example of September 29, 1994, is characterised by a relatively moderate but continuous level of $I_{\max}$, with several secondary maxima and $I_{\max}$ slightly exceeding 4.0 mm/5 min along approximately 150–160 min after the beginning of the episode. These characteristics would be in agreement with the profile of intensity recorded on the gauge number 2 of the urban network. The example of October 17, 1999, is characterised by low values of $I_{\max}$ except for the beginning of the episode (elapsed time close to 20 min and a maximum exceeding 5.5 mm/5 min) and the absolute maximum (a notable value exceeding 11.0 mm/

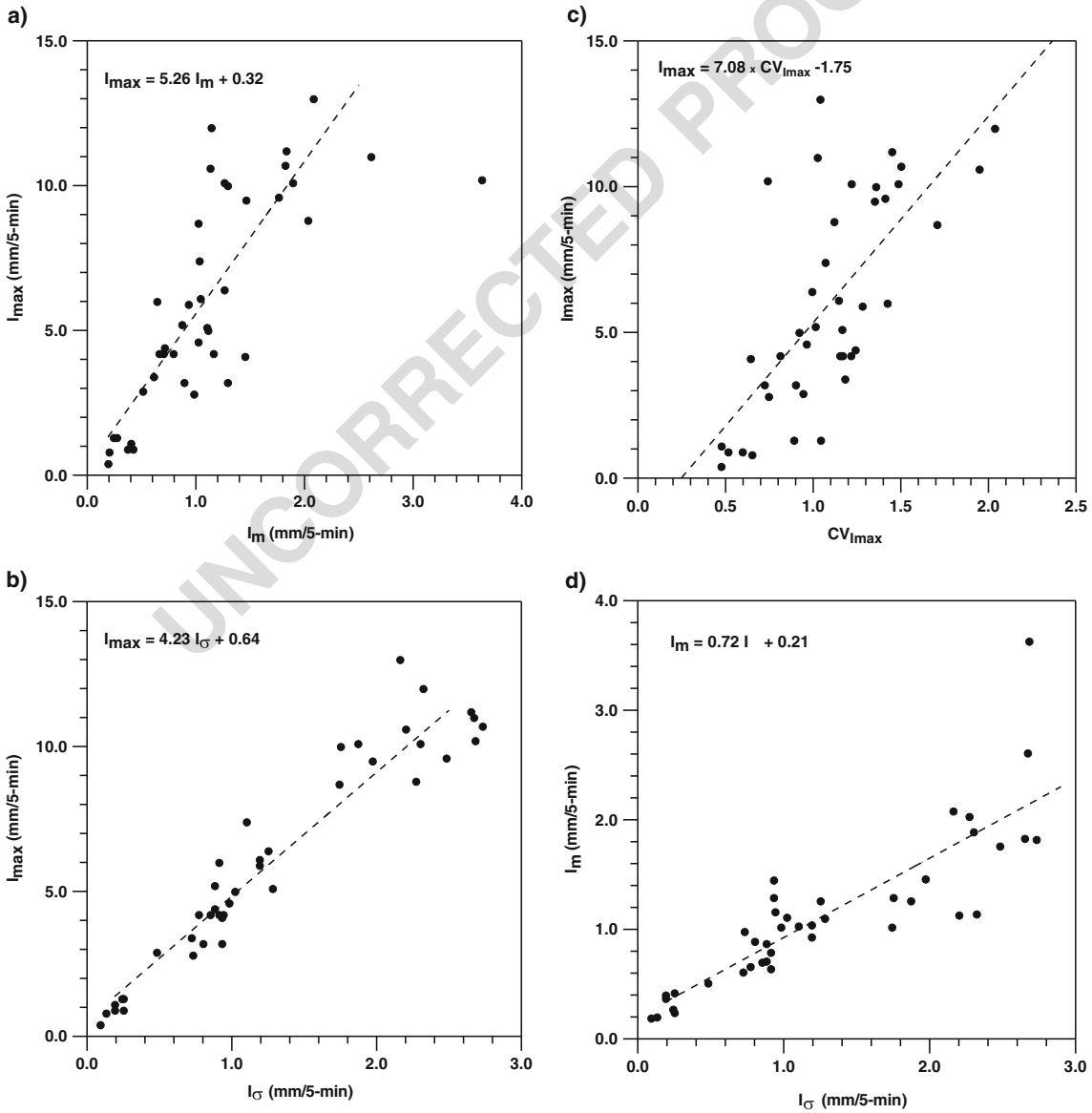

Fig. 8 Dependence of the maximum 5-min rain amount, $I_{\max}$, for every episode on **a** the average intensity, I_m; **b** the standard deviation, I_σ and **c** the coefficient of variation, CV_{Imax}. **d** Relationship between I_m and I_σ

UNCORRECTED PROOF

AUTHOR'S PROOF!

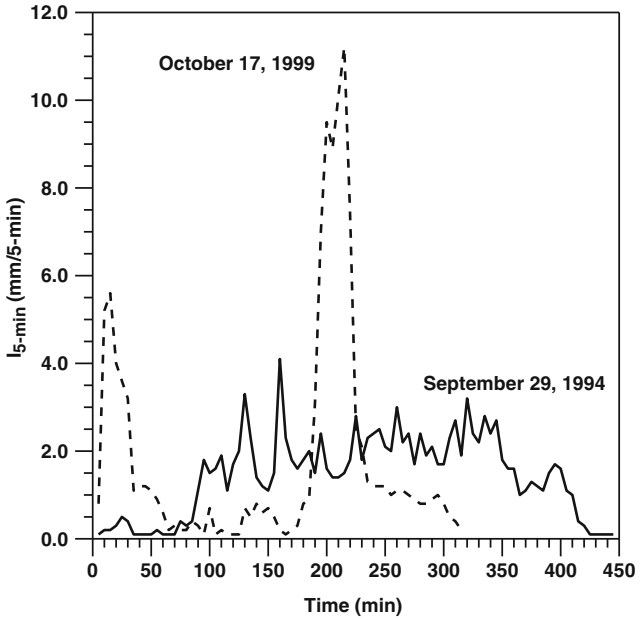

Fig. 9 Two examples of 5-min profiles on the *September 29, 1994*, and on the *October 17, 1999*, episodes

5 min for an elapsed time of approximately 210 min). This profile would agree with that of rain rate gauge number 1. Nevertheless, the early I_{max} observed in Fig. 9 is not detected in rain rate gauge number 1. This lack of recorded peaks could be a consequence of time shifts on the starting time of the rainfall episodes at the different rain rate gauges. In agreement with Fig. 1, and mentioned in Sect. 2, the urban network covers a non-negligible area of approximately 100 km^2. The size of this area would be sufficient to distinguish time shifts among rain rate gauges, a consequence of several atmospheric dynamic processes, such as eastern advections, frontal passages or convective phenomena.

For a better description of the profiles shown in Fig. 9, the time evolution and the spatial propagation of the outstanding peaks detected for September 29, 1994, and October 17, 1999, episodes are shown in Fig. 10. Given that September 29, 1994, is characterised by a set of relatively similar intensity peaks, the spatiotemporal evolution has been analysed for 5-min intervals covering two lengths of 55 min after the beginning of the episode. In this way, several peaks close to 3.0 mm/5 min and another slightly exceeding 4.0 mm/5 min can be detected. Figure 10a describes the track of I_{max} for the first chosen length of 55 min. I_{max} are displaced from north-east to south-west of the Barcelona urban area, with signs of a clockwise rotation of maxima emplacements, with a moderate I_{max} being detected, slightly exceeding 3.0 mm/5 min. It is worth mentioning that, at the same time that intensity peaks moved towards south-west, 5-min amounts close to the littoral are null. All these patterns would suggest an eastern advection process in agreement with surface pressure and 500-hPa charts. I_{max} maps for the other length of 55 min (Fig. 10b) depict a not-so-clear track. Nevertheless, signs of a counter-clockwise trajectory of I_{max} can be detected. It is also worth mentioning that I_{max} only exceed 3.0 mm/5 min for a short period and a very small area in the coast line. Additionally, as for the length described in Fig. 9a, nuclei of I_{max} occupy places in the urban network spatially opposed to those corresponding to null or almost null 5-min rain amounts. In short, patterns derived from both figures could be two pictures of spatial rainfall distribution generated by an eastern advection favoured by relatively cold air masses in altitude, in agreement with surface and 500-hPa charts.

Figure 10c, d describes the evolution of the two intensity peaks detected in Fig. 9 for October 17, 1999. The first one is monitored at 5-min intervals, being clearly observed that the nucleus of outstanding rainfall intensity arrives from the south and in a few minutes achieves its highest value (exceeding 5.0 mm/5 min). Just after, this nucleus shifts parallel to the coast line, splitting later into two nuclei of notably lower intensity. These nuclei follow different tracks towards the north-west (littoral chain) and the north-east along the coast line. In agreement with synoptic surface and 500-hPa charts, the evolution of this nucleus of rainfall intensity would correspond to a convective process characterised by short periods (about 25–30 min) of notable intensity. This hypothesis would be reinforced by Fig. 10d, where the track of a second peak of intensity is monitored. The scheme is quite similar to that of Fig. 10c. The track of the intensity peak nucleus is very similar and the length is again close to 25–30 min. Nevertheless, the highest intensity is achieved in this second track at the end of the process, but not at the beginning, close to 11.0 mm/5 min, with outstanding high values all along the track. These patterns would not be contradictory in comparison with those observed for the first nucleus. Two consecutive convective cells, with a time delay between them of a few minutes, similar tracks and lengths, and belonging to the same episode, but with quite different rain, can be explained as a consequence of similar atmospheric conditions of previous cases.

Another remarkable example of rainfall episode is shown in Fig. 10e. Surface and 500-hPa charts strongly suggest that this episode corresponds to a typical summer storm, characterised by heavy rainfall amount (close to 60 mm), localised high intensity along 30 min and with a W-E trajectory. In contrast with the two previous episodes of Fig. 10a–d, maximum intensity values from 11.0 to 12.0 mm/5 min are detected along a short period of 20–30 min. Although nuclei of high intensity do not cover the entire urban domain, this kind of episode could be associated with flood risks due to their outstanding intensities.

UNCORRECTED PROOF

AUTHOR'S PROOF!
JmlID 704_ArtID 2193_Proof# 1 - 11/06/2017

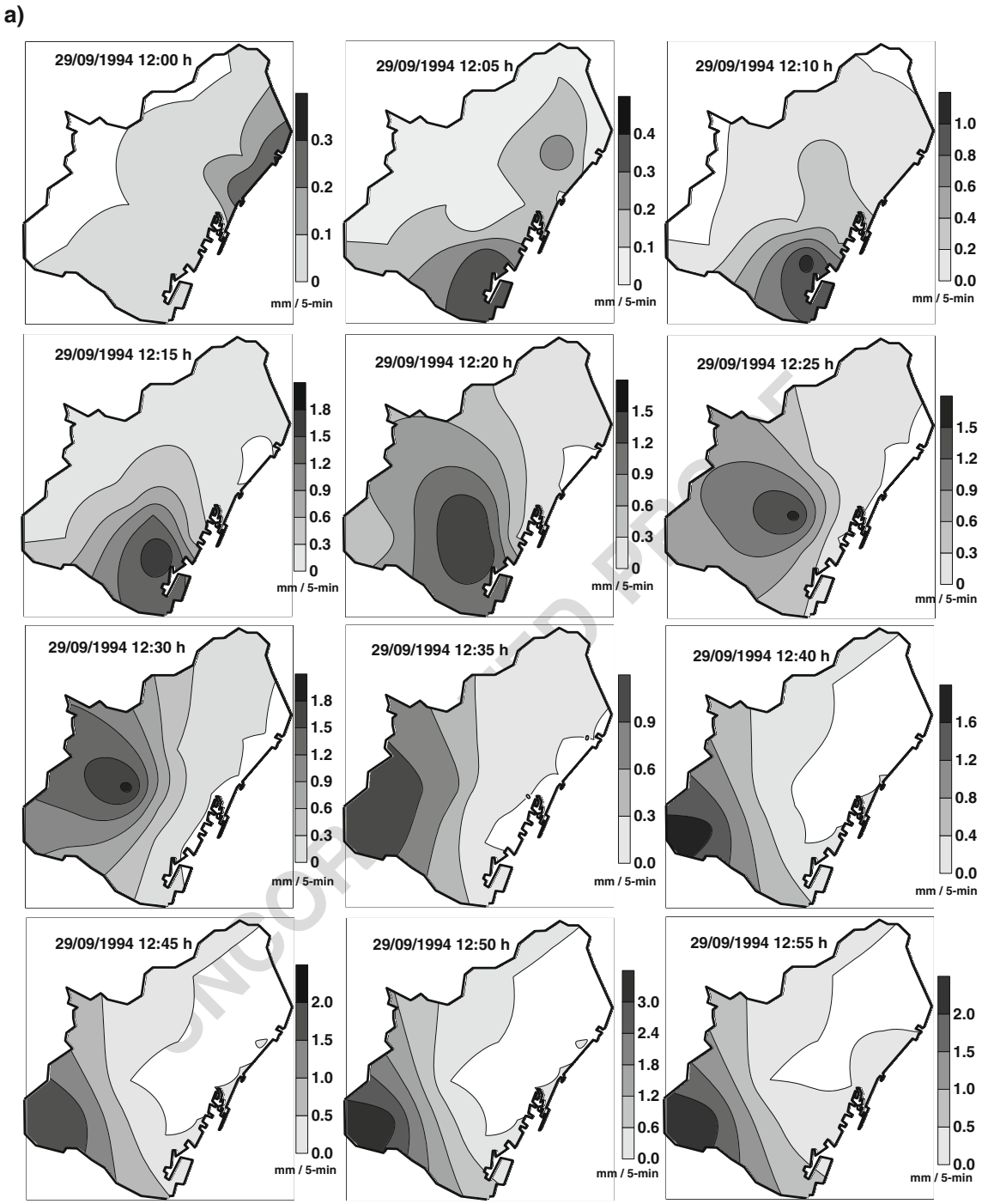

Q13 **Fig. 10** Spatiotemporal evolution of the 5-min rain amounts recorded in the urban network on **a**, **b** *September 29, 1994*, and **c**, **d** *October 27, 1999*. *Isolines* are given in mm/5 min

Finally, the absolute maximum of 5-min rain amounts recorded at every one of the 23 rain gauges along 1994–2009 is shown in Fig. 11. In spite of the relatively small dimension of the analysed area, the distribution of maxima intensities is not homogeneous. Whereas absolute maximum intensity varies from 10.0 to 13.0 mm/5 min for a great part of the area, three nuclei reaching or slightly exceeding 19.0 mm/5 min are found. These three nuclei and surrounding areas should be taken into account with the aim of preventing the generation of floods caused by very high intensities. Even though these results concerning spatial distribution of high intensities are based on a short recording period of 16 years, signs of flood risk become evident. In order to quantify this kind

AUTHOR'S PROOF!

b)

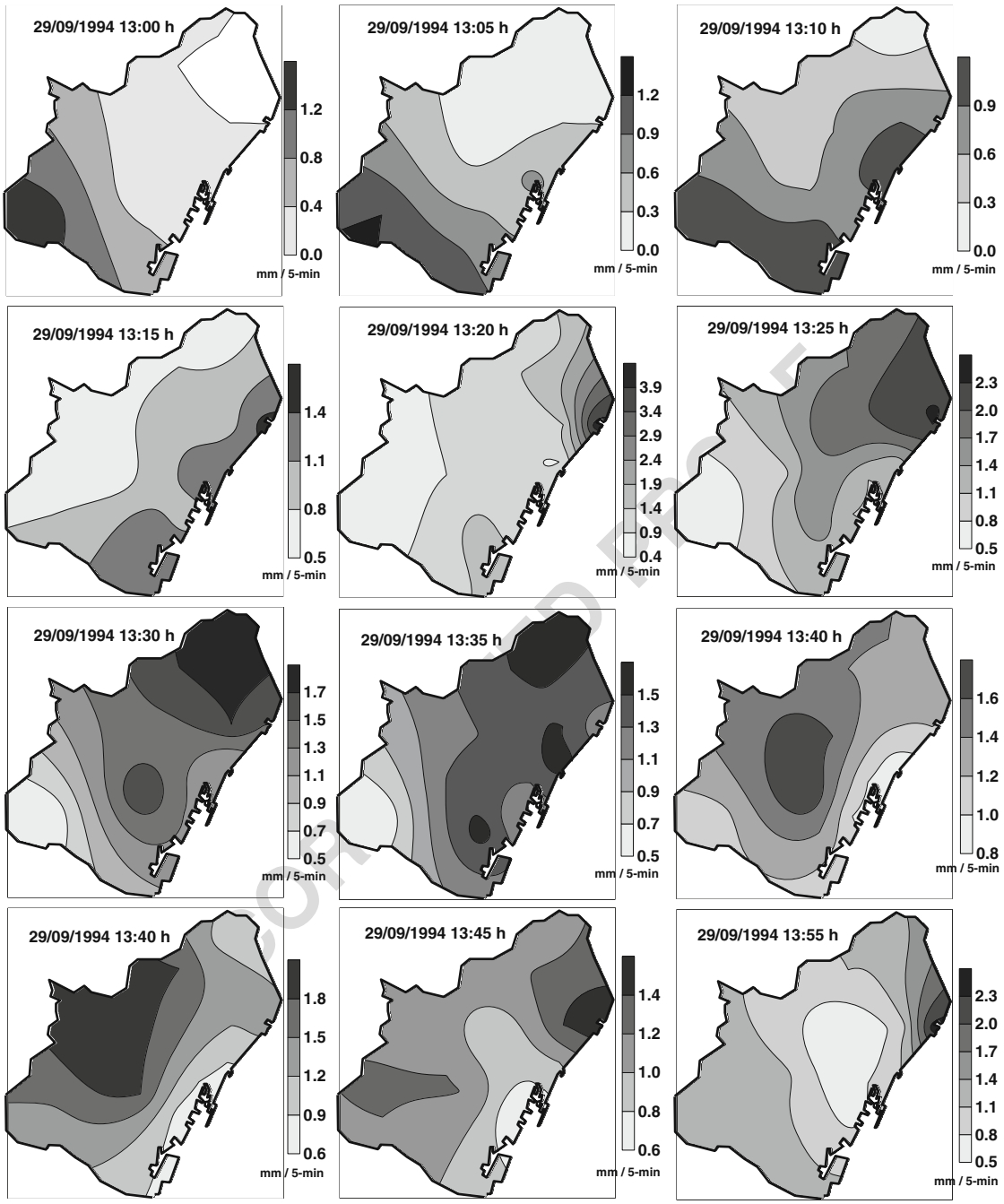

Fig. 10 (continued)

of risk, a future step should be an analysis of 5-min amount extremes, including statistical models, return periods and spatial distribution of extremes. This strategy would take advantage of an increased number of samples for the same recording period, because rainfall episodes would not be restricted to those with lengths longer than 2 h. Conversely, all 5-min amounts would contribute to obtain reliable series of empiric extremes.

5 Conclusions

The concept and mathematical formulation of NIC has been applied to analyse 41 selected rain rate episodes in an urban network, related to different synoptic situations, with different lengths and rain amounts, from the viewpoint of 5-min amounts. In contrast with the dependence of NRC on the coefficient of variation of the series (daily and monthly

AUTHOR'S PROOF!
JnlID 704_ArtID 2193_Proof# 1 - 11/06/2017

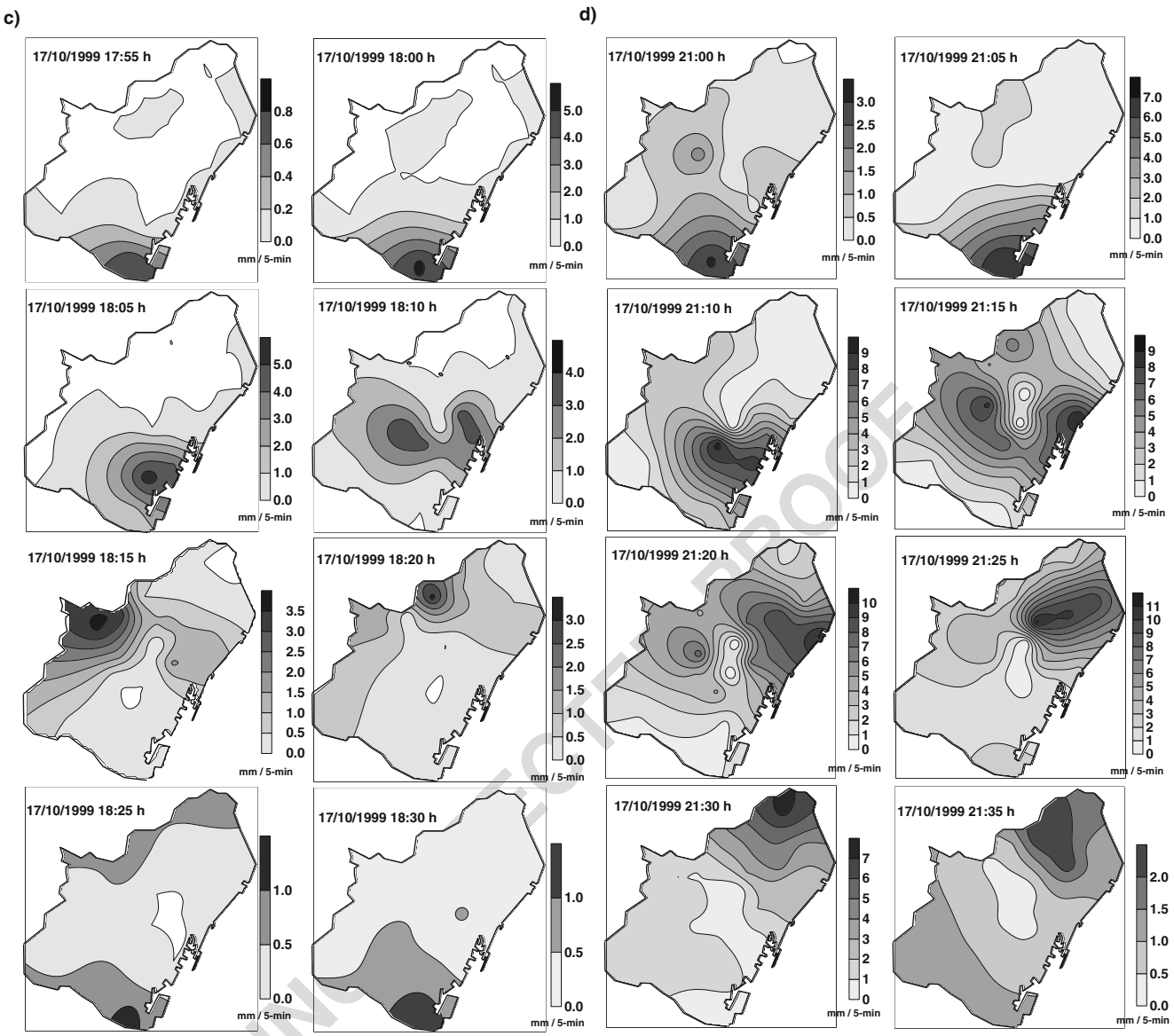

Fig. 10 (continued)

amounts, for instance), the NICs are clearly described by power laws characterised by their exponents κ. Nevertheless, some signs of dependence of κ on CV_I are also detected. In consequence, NICs are also in some way governed by the CV_I or, in other words, by the spreading of 5-min rain amounts.

It is also worthy of mention that the power laws exclude 5-min rain amounts below the resolution of rain rate gauges, due to intermittencies in the rainfall episode. As a result of all these characteristics of the NIC and the power law properties, seven parameters have been finally assumed, describing a specific rain rate episode. On the one hand, two of them, R and L, are basic. On the other hand, the intermittency parameter Y_0 and the coordinates (X_m,Y_m) are three new parameters. Even though certain relationships may be detected between them, κ and CV_I should be considered as different parameters. The mentioned relationship is not a mathematical function exactly relating them, but just suggesting a decreasing evolution of κ with CV_I modelled by an exponential law. The other relationships between pairs of different parameters also contribute to a better knowledge of the relationship among different features of the rainfall episodes. These relationships can be interpreted as increasing/decreasing tendencies on one parameter when this is compared with increasing/decreasing values of another, but not as an accurate and exact dependence of one parameter on another. Nevertheless, it is worth mentioning that whatever the rain amount, length and synoptic chart associated with a rainfall episode, the same relationships between pairs of parameters are valid for the 41 episodes. This result is outstanding, taking into account that these episodes belong to the four seasons and they are due to such varied processes as eastern advections, frontal passages or convective phenomena.

AUTHOR'S PROOF!

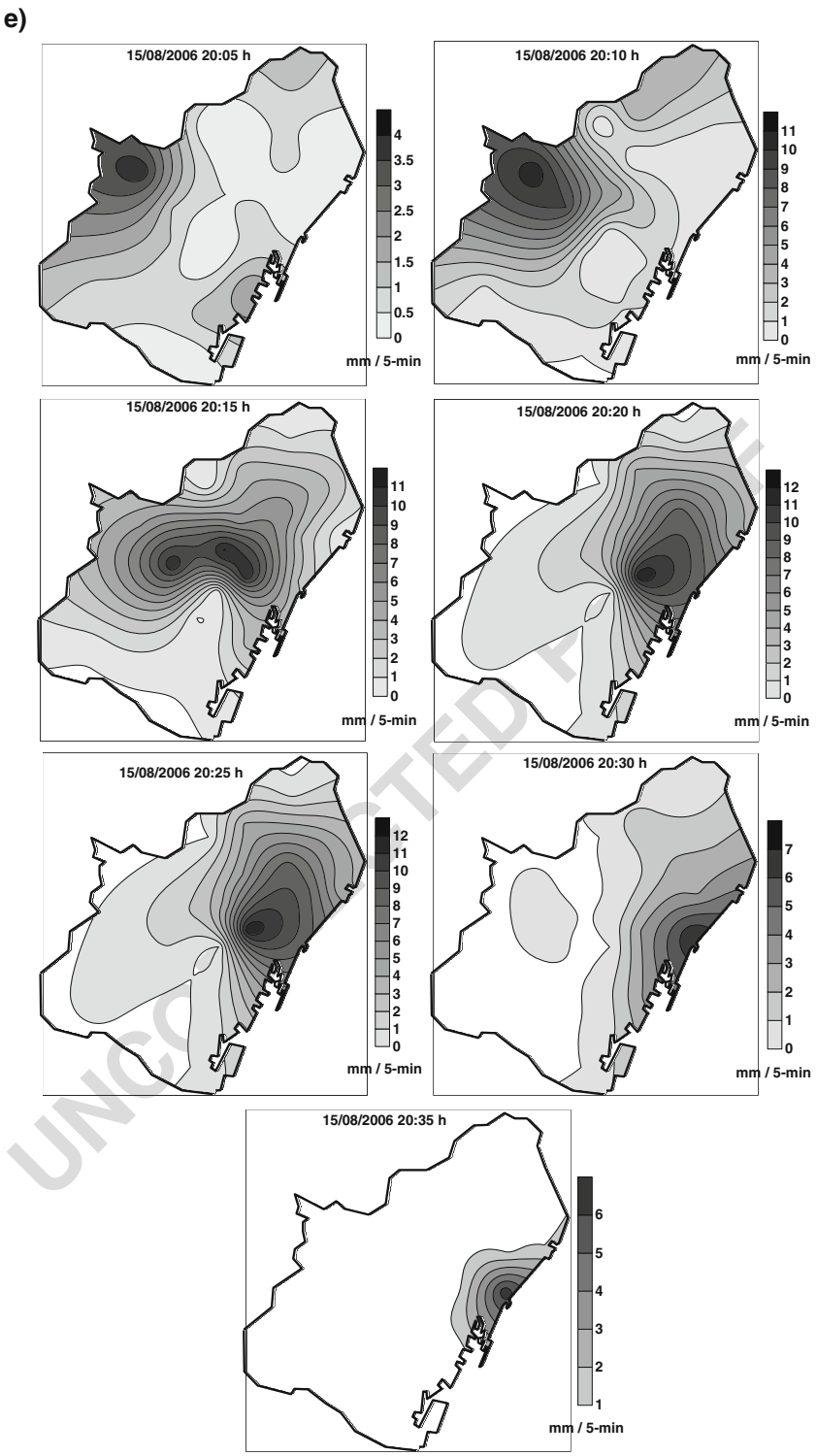

Fig. 10 (continued)

From the viewpoint of flood prevention, taking into account some geographical and topographical characteristics of Barcelona area (closeness to the Mediterranean coast line, enhancement of rainfall intensity due to the vicinity of the littoral chain and a smooth slope from this chain to the littoral coast), characteristics derived from analyses of extreme 5-min rain amounts are valuable. Specifically, dependences of I_{max} on I_m and I_σ offer a picture of expected extreme intensities for smooth, moderate and heavy intensity episodes, as well as the increase of I_{max} for episodes of wide intensity range. Additionally, the time evolution of three episodes shown in Fig. 10a–e could be an example of valuable information

AUTHOR'S PROOF!

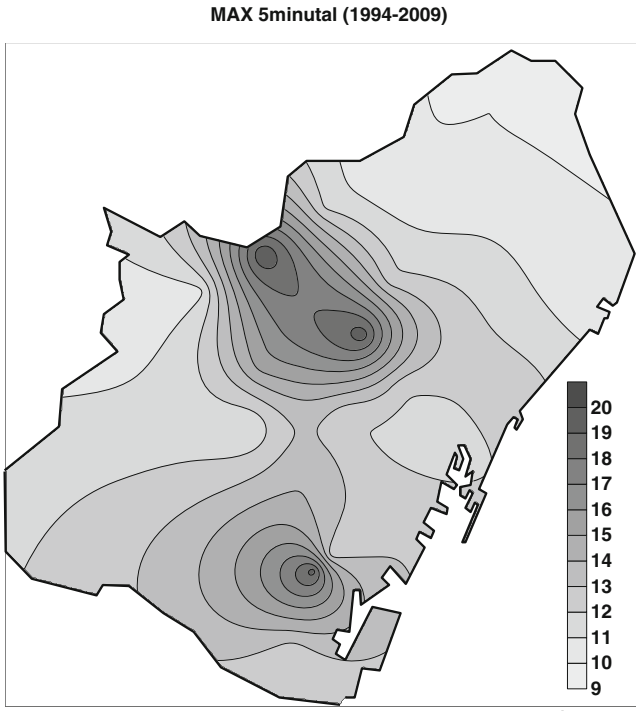

Fig. 11 Spatial distribution of the maximum 5-min rain amounts recorded in the urban network for years 1994–2009. *Isolines* are given in mm/5 min

obtained by the spatial–temporal monitoring of episodes recorded by the urban network. Results associated with Fig. 11 are also very important. For future flood episode prevention, two relevant questions should be considered. First, as mentioned before, the spatial distribution of I_{max} is not homogeneously spread, but concentrated around three nuclei of outstanding values. And second, even for places away from these three critical points, 5-min rain amounts are not negligible. High magnitudes on a metropolitan area, as those exceeding 10 mm/5 min, should be carefully taken into account in engineering studies, leading to a reduction of flood risk and its effects. Alternatively, flood risks could be also quantified by means of extreme value statistics and return periods. This kind of analysis is out of the scope of this paper, but it should be a forthcoming objective for a better contribution to mitigate the effects of heavy rainfall episodes on urban areas.

A simple analysis at the daily scale is not sufficient to improve drainage systems, especially for western Mediterranean areas, where heavy and irregular rainfalls are expected. A more detailed knowledge about short integration-time records, as 5-min amounts, is convenient to design right-dimensioned drainages submitted to heavy short-length rainfall intensities, which may generate outstanding flows. In particular, NIC permits the determination for every rain rate gauge or for every episode the probability of exceeding a certain 5-min amount, the expected I_{max} and where the highest I_{max} are expected, permitting then a more accurate design. For instance, in agreement with Fig. 11, the nucleus of high I_{max} close to the Barcelona harbour is on the windward side of a low hill of 150 m a.s.l. (Fig. 1). This fact possibly enhances the effects of eastern and south-eastern advections. The other nuclei of extreme I_{max} appear very close to the littoral chain (500 m a.s.l.), and very likely, the same causes concerning eastern advections proposed for the first nucleus would be right now.

Finally, it is also worthy of mention that the fractal structure of the rainfall intensity is clearly manifested by the power law describing NIC, as well as by the established power law relationships between pairs of parameters (Y_m,R), and (X_m,R). These fractal relationships should be in agreement with the fractal scaling behaviour of rainfall intensities.

Acknowledgements The rain rate gauge network data has been gently provided by CLABSA, the company that controlled the sewer systems of Barcelona along the years 1994–2009.

References

Alijani B, O'Brien J, Yarnal B (2008) Spatial analysis of precipitation intensity and concentration in Iran. Theor Appl Climatol 94:107–124

Ananthakrishnan R, Soman MK (1989) Statistical distribution of daily rainfall and its association with the coefficients of variation of rainfall series. Int J Climatol 9:485–500

Benjamin JR, Cornell CA (1970) Probability, statistics and decision for civil engineers. McGraw-Hill, New York 685 pp

Burgueño A, Austin J, Vilar E, Puigcerver M (1987) Analysis of moderate and intense rainfall rates continuously recorded over half a century and influence on microwave communications planning and rain-rate data acquisition. IEEE Trans on Comm 35:382–395

Burgueño A, Puigcerver M, Vilar E (1988) Influence of rain gauge integration time on the rain rate statistics used in microwave communications. Ann Télécommun 43:522–527

Burgueño A, Vilar E, Puigcerver M (1990) Spectral analysis of 49 years of rainfall rate and relation to fade dynamics. IEEE Trans Commun 38:1359–1366

Burgueño A, Serra C, Lana X (2004) Monthly and annual statistical distributions of the daily rainfall at the Fabra Observatory (Barcelona, NE Spain) for the years 1917-1999. Theor Appl Climatol 77:57–75

Burgueño A, Martínez MD, Lana X, Serra C (2005) Statistical distributions of the daily rainfall regime in Catalonia (NE Spain) for the years 1950-2000. Int J Climatol 25:1381–1403

Burgueño A, Martínez MD, Serra C, Lana X (2010) Statistical distribution of daily rainfall regime in Europe for the period 1951-2000. Theor Appl Climatol 102:213–226

Casas MC, Codina B, Redaño A, Lorente J (2004) A methodology to classify extreme rainfall events in the western Mediterranean area. Theor Appl Climatol 77:139–150. doi:10.1007/s00704-003-0003-x

Casas MC, Rodríguez R, Redaño A (2010) Analysis of extreme rainfall in Barcelona using a microscale rain gauge network. Meteorol Appl 17:117–123. doi:10.1002/met.166 http://hdl.handle.net/2117/6733

Casas MC, Rodríguez R, Prohom M, Gázquez A, Redaño A (2011) Estimation of the probable maximum precipitation in Barcelona (Spain). Int J Climatol 31:1322–1327. doi:10.1002/joc.2149 http://hdl.handle.net/2117/9654

UNCORRECTED PROOF

AUTHOR'S PROOF!

Hosking JRM, Wallis JR (1997) Regional frequency analysis. Cambridge University Press, Cambridge 224 pp

Hosking JRM, Wallis JR, Wood EF (1985) Estimation of the generalised extreme value distributions by the method of probability-weighted moments. Techtonometrics 27:251–261

Jolliffe IT, Hope PB (1996) Representation of daily rainfall distributions using normalised rainfall curves. Int J Climatol 16:1157–1163

Lana X, Serra C, Burgueño A (2003) Trends affecting pluviometric indices at the Fabra Observatory (Barcelona, NE Spain) from 1917 to 1999. Int J Climatol 23:315–332

Lana X, Martínez MD, Serra C, Burgueño A (2005) Periodicities and irregularities of indices describing the daily pluviometric regime of the Fabra Observatory (NE Spain) for the years 1917-1999. Theor Appl Climatol 82:183–198

Lorente J, Redaño A (1990) Rainfall rate distribution in a local scale: the case of Barcelona City. Theor Appl Climatol 41:23–32

Malamud BD, Turcotte DL (1999) Self-affine time series: generation and analyses. Adv Geophys 40:1–90

Martínez MD, Lana X, Burgueño A, Serra C (2012) Normalized monthly shortage curves: a contribution for a better understanding of monthly rainfall deficit in Western Europe. Theor Appl Climatol 108:535–552

Martín-Vide J (2004) Spatial distribution of a daily precipitation concentration index in Peninsular Spain. Int J Climatol 24:959–971

Monjo R, Martin-Vide J (2016) Daily precipitation concentration around the world according to several indices. Int J Climatol. doi:10.1002/joc.4596

Rodríguez R, Navarro X, Casas MC, Redaño A (2013a) Rainfall spatial organization and areal reduction factors in the metropolitan area of Barcelona (Spain). Theor Appl Climatol 114:1–8. doi:10.1007/s00704-012-0818-4 http://hdl.handle.net/2117/17169

Rodríguez R, Casas MC, Redaño A (2013b) Multifractal analysis of the rainfall time distribution on the metropolitan area of Barcelona (Spain). Meteorog Atmos Phys 121(3–4):181–187. doi:10.1007/s00703-013-0256-6 http://hdl.handle.net/2117/19110

Rodríguez-Solà R, Casas-Castillo MC, Navarro X, Redaño A (2016) A study of the scaling properties of rainfall in Spain and its appropriateness to generate intensity-duration-frequency curves from daily records. Int J Climatol doi. doi:10.1002/joc.4738 http://hdl.handle.net/2117/87312

Soman MK, Krishna KK (1990) Some aspects of daily rainfall distribution over India during the south-west monsoon season. Int J Climatol 10:299–311

Vilar E, Burgueño A (1991) Analysis and modelling of time intervals between rain rate exceedances in the context of fade dynamics. IEEE Trans Commun 39:1306–1312

Vilar E, Burgueño A, Puigcerver M, Austin J (1988) Analysis of joint rainfall rate and duration statistics: microwave system design implications. IEEE Trans Commun 36:650–661

UNCORRECTED PROOF